

Article

Dynamics of the Creation of a Rotating Bose–Einstein Condensation by Two Photon Raman Transition Using a Laguerre–Gaussian Laser Pulse

Koushik Mukherjee ^{1,*}, Soumik Bandyopadhyay ^{2,3,†}, Dilip Angom ², Andrew M. Martin ⁴
and Sonjoy Majumder ¹

- ¹ Indian Institute of Technology Kharagpur, Kharagpur 721302, West Bengal, India; sonjoym@phy.iitkgp.ac.in
² Physical Research Laboratory, Ahmedabad 380009, Gujarat, India; soumik@prl.res.in (S.B.); angom@prl.res.in (D.A.)
³ Indian Institute of Technology Gandhinagar, Palaj, Gandhinagar 382355, Gujarat, India
⁴ School of Physics, University of Melbourne, Melbourne, VIC 3010, Australia; martinam@unimelb.edu.au
* Correspondence: koushikphysics21@gmail.com
† Current address: INO-CNR BEC Center and Department of Physics, University of Trento, Via Sommarive 14, 38123 Trento, Italy.

Abstract: We present numerical simulations to unravel the dynamics associated with the creation of a vortex in a Bose–Einstein condensate (BEC), from another nonrotating BEC using two-photon Raman transition with Gaussian (G) and Laguerre–Gaussian (LG) laser pulses. In particular, we consider BEC of Rb atoms at their hyperfine ground states confined in a quasi two dimensional harmonic trap. Optical dipole potentials created by G and LG laser pulses modify the harmonic trap in such a way that density patterns of the condensates during the Raman transition process depend on the sign of the generated vortex. We investigate the role played by the Raman coupling parameter manifested through dimensionless peak Rabi frequency and intercomponent interaction on the dynamics during the population transfer process and on the final population of the rotating condensate. During the Raman transition process, the two BECs tend to have larger overlap with each other for stronger intercomponent interaction strength.

Keywords: Bose–Einstein condensate; Laguerre–Gaussian; Raman transition; cold atoms; light–matter interaction; particle transfer; density pattern



Citation: Mukherjee, K.; Bandyopadhyay, S.; Angom, D.; Martin, A.M.; Majumder, S. Dynamics of the Creation of a Rotating Bose–Einstein Condensation by Two Photon Raman Transition Using a Laguerre–Gaussian Laser Pulse. *Atoms* **2021**, *9*, 14. <https://doi.org/10.3390/atoms9010014>

Received: 10 January 2021
Accepted: 4 February 2021
Published: 8 February 2021

Publisher’s Note: MDPI stays neutral with regard to jurisdictional claims in published maps and institutional affiliations.



Copyright: © 2021 by the authors. Licensee MDPI, Basel, Switzerland. This article is an open access article distributed under the terms and conditions of the Creative Commons Attribution (CC BY) license (<https://creativecommons.org/licenses/by/4.0/>).

1. Introduction

Creation of vortex states in atomic Bose–Einstein condensates (BECs) has been the subject of quite intensive research, with particular focus on superfluid properties [1–3] and quantum turbulence [4–10]. A number of theoretical and experimental studies have considered the properties of vortex states in single and multicomponent BECs [11–16], their stability [17–24] and collective excitations [25–29], thus opening up an avenue of opportunities to explore and develop quantum state engineering in a macroscopic system [21,30,31]. Owing to the highly controllable state-of-the-art BEC experiments, the presence of a vortex in BECs can be detected and their dynamics can be monitored with good spatial and temporal resolution [31–36]. Numerous techniques, which mainly rely upon two distinct physical situations, have been proposed theoretically [37–44] and developed experimentally [45–48] to generate vortices in BECs. In rotating traps, vortices are the thermodynamic ground states with quantized angular momentum, but in stationary traps, the creation of vortices requires other dynamical means. Various methods to create vortices include the perturbation of the system with a time-dependent boundary. In particular, such time-dependent boundaries can be created either by moving a blue detuned laser through the condensate [43,49] or by rotating the trap anisotropy [46]. In the other scheme, the so-called phase imprinting technique [37,42,45,50–54], one can engineer the macroscopic

wavefunctions of BECs by coupling the internal atomic levels with either an optical field or a magnetic field. Remarkably, the topological phase pattern of the coupling field is imprinted into the condensate wavefunctions. This topological phase, which is independent of the field strength, is uniquely determined by the spatial structure of the coupling field.

The helical phase front of Laguerre–Gaussian (LG) laser beams has been associated with its orbital angular momentum (OAM) in the paraxial regime [55]. A photon of such an LG laser modes has phase profile $e^{il\phi}$, and carries $l\hbar$ unit OAM in the transverse plane, where ϕ is the angular coordinate and l is an integer, known as the winding number of the beam. Such LG modes are known to transfer OAM from an optical field to the Rydberg atom [56], BECs [57–60], and to create a mechanical rotation of particles [61,62]. It was shown that a coherent coupling between the ground state of condensate with a rotating condensate in vortex state, can be achieved by the transfer of OAM of photons to the condensed atoms through Raman transitions [37]. Quantum dynamics of such vortex coupler using LG beam was studied, and an off-axis motion of the quantized vortex cores was interpreted as the collapse and revival of the atoms of the condensate [63]. Besides, a pair of LG laser modes with unequal phase windings couple internal atomic states of BEC through Raman transitions, and thus giving rise to spin and orbital angular momentum coupling in the ground states of a spinor BEC [64,65]. Moreover, it has been shown that almost all the atoms in the non-rotating BEC can be transferred to the BEC with vortex, by employing LG beams [66,67].

Although an impressive volume of literature has been devoted to this subject, few of its vital aspects remain further to be explored. One such aspect constitutes the role played by the interaction between two BEC components on the population transfer. Indeed, during the transfer process, atoms of two condensates are present in two different hyperfine states, one with vorticity and another without vorticity. Thus, not only the atom–laser coupling, but also the atom–atom interaction between two different components is expected to influence the population transfer process. Note that the focus of the majority of the previous studies has been on the complete particle transfer from one quantum state to another. However, it is expected that by maneuvering atom–light coupling and inter-component interaction one could achieve a population transfer of any desired value. In this way it equips us to realize a binary-mixture where one component contains a vortex, and the other does not, thus emulating the so-called vortex-bright-soliton structure [16,68]. Additionally, it is also desirable to know, through the miscibility parameter [15,69,70], how atoms in the condensate with a vortex penetrate into atoms of the condensate without any vortex during the transfer process [15,69,70]. Therefore, motivated by experimental accessibility [71,72] and theoretical novelty of the problem, we theoretically address these important aspects of the transfer mechanism in this paper.

We investigate the dynamics of population transfer from a nonrotating BEC to a Raman coupled rotating BEC by employing LG and Gaussian (G) pulses. In this process, the atoms in rotating BEC gain angular momentum from the LG laser pulse. We consider pulsed G and LG beams as the pump and Stokes beams, respectively, to transfer the atoms from one hyperfine level to another. In particular, we choose the temporal width of the pulses to be in the same time scale determined by the trap frequency. This consideration provides us the framework to understand the dynamics during the transfer process. Numerically integrating the Raman coupled multicomponent Gross-Pitaevskii equations, we point out the following key points: (i) the sign of the vorticity of the condensate as well as the initial growth region of the vortex state, captured within the density patterns, depend upon which laser mode is chosen as pump or Stokes beam and (ii) the repulsive inter-component atomic interaction and peak Rabi frequency of laser beams determine the number of atoms transferred to the non-rotating BEC. By calculating the overlap integral between the two condensates we also quantify how two condensates penetrate into each other during the transfer process.

We have organized the remainder of this paper as follows. In Section 2 we describe the theory of transfer mechanism. Section 3 provides a brief description of the numerical

schemes used. In Section 4 we present results of the complete particle transfer and effects of the inter-particle interactions and the Raman coupling parameter on the final population of the rotating BEC. In Section 5, we discuss the implication and possible future extensions associated with the results presented. Appendix A presents the effects of trap frequencies and the time-delay between the pulses on the population transfer. Finally, in Appendix B we briefly outline the Hamiltonian and the derivation of the equations of motions.

2. Theoretical Methods

In our study, we consider BEC of alkali atoms trapped in a quasi two-dimensional harmonic trap confined in the $x - y$ plane with z axis being the quantization axis. In order to transfer OAM from the optical beam to the BEC, we consider three electronic levels of the alkali atoms are coupled by a pair of laser pulses in Λ -type configuration as shown in Figure 1. Atoms of initially prepared BEC are at the state $|1\rangle$, one of the hyperfine levels of the electronic ground state of atoms. The state $|3\rangle$ is an intermediate non-resonant excited state. The final state is considered to be $|2\rangle$, another hyperfine level of the electronic ground state of the atoms. The atoms are irradiated by two laser pulses propagating collinearly parallel to the quantization axis [73]. We remark that with the dipole approximation of the atomic transitions, the changes in the internal spin states of atoms are dictated by polarizations of two light fields. However, the changes in external orbital motion of the atoms of BEC around the quantization axis are determined by the difference of the orbital angular momentum (OAM) of two light fields [57]. Let us consider that the OAM of the twisted laser pulses for the transition from state $|1\rangle$ to state $|3\rangle$ is l_1 and for $|3\rangle$ to $|2\rangle$ transition is l_2 . Then, the electric field vectors involved in this absorption or emission transitions can be written as (for $i = 1$ and 2)

$$\mathbf{E}_i(x, y, t) = \hat{\epsilon}_i \mathcal{E}_i(t) (x^2 + y^2)^{\frac{|l_i|}{2}} e^{-\frac{(x^2+y^2)}{w_i^2}} e^{-i(k_i z - \omega_i t)}, \quad (1)$$

where $\mathcal{E}_i(t)$, $\hat{\epsilon}_i$, k_i and ω_i are the corresponding time dependent amplitude profile, polarization vector, wave number and frequency of the i -th pulse, respectively. We consider the temporal amplitude profiles of both pulses have the same form [74]:

$$\mathcal{E}_{1(2)}(t) = \mathcal{E}_{\max} e^{-\left(\frac{t-\tau_{1(2)}}{T}\right)^2}, \quad (2)$$

where $\tau_{1(2)}$ is the temporal position of the peak value of electric field $\mathcal{E}_{1(2)}$. Maximum amplitude \mathcal{E}_{\max} and pulse duration T are the same for both pulses. The optical absorption-emission cycle imparts OAM onto the atoms in final state $|2\rangle$ and creates a vortex in the BEC with charge $(l_1 - l_2)$ unit. Because of collinearity of the E_1 and E_2 pulses, no additional linear momentum is generated in the final state. In addition to such two-photon transitions in atomic BEC, these lasers also create extra confining potential, namely optical dipole potentials for the atoms in the states $|1\rangle$ and $|2\rangle$ [75]. In practice the value of detuning Δ is large, which ensures the negligible populations in state $|3\rangle$. This allows us to eliminate the state $|3\rangle$ adiabatically. During the transfer process, atoms are present in both the hyperfine states, $|1\rangle$ and $|2\rangle$. Therefore, coherent evolution of the condensates of atoms in these two states, characterized by wavefunctions $\Psi_1(x, y, t)$ and $\Psi_2(x, y, t)$ respectively, are governed by two Raman coupled Gross-Pitaevskii equations (see Appendix B for the derivation)

$$i \frac{\partial \Psi_1}{\partial t} = \left[-\frac{1}{2} \nabla_{\perp}^2 + \frac{r^2}{2} + \sum_j \mathcal{G}_{1j} |\Psi_j|^2 + \mathcal{V}_1(t) r^{2|l_1|} e^{-\frac{2r^2}{w_1^2}} \right] \Psi_1 + \mathcal{V}'(x, y, t) \Psi_2 e^{-i(l_1 - l_2)\phi}, \quad (3)$$

and,

$$i \frac{\partial \Psi_2}{\partial t} = \left[-\frac{1}{2} \nabla_{\perp}^2 + \frac{r^2}{2} + \sum_j \mathcal{G}_{2j} |\Psi_j|^2 + \mathcal{V}_2(t) r^{2|l_2|} e^{-\frac{2r^2}{w_2^2}} \right] \Psi_2 + \mathcal{V}'(x, y, t) \Psi_1 e^{i(l_1 - l_2)\phi}, \quad (4)$$

where $r^2 = x^2 + y^2$, $\mathcal{V}' = \sqrt{\mathcal{V}_1 \mathcal{V}_2} (r^2)^{(|l_1|+|l_2|)/2} \exp[-2r^2(1/w_1^2 + 1/w_2^2)]$, and $\mathcal{V}_{1(2)}(t) = \mathcal{V}_{\max} \exp[-(t - \tau_{1(2)})^2/T^2]$ with $\mathcal{V}_{\max} = \mathcal{E}_{\max}^2 d^2 / \hbar^2 \omega \Delta$. \mathcal{E}_{\max} is maximum light intensity of both pulses and d is the atomic transition dipole moment and $w_{1(2)}$ is the beam waist of the corresponding laser pulse. Therefore, the effective trap potentials felt by atoms of the condensates are

$$V_{\text{eff},1(2)} = \frac{r^2}{2} + \mathcal{V}_{1(2)}(t) r^{2|l_1|(|l_2|)} e^{-\frac{2(r^2)}{w_{1(2)}^2}}. \tag{5}$$

We derive Equations (3) and (4) by nondimensionalizing Equations (A11) and (A12) respectively. For this, we scale the spatial coordinates by oscillator length $a_{\text{osc}} = \sqrt{\hbar/m\omega}$, time by $1/\omega$ and condensate wavefunctions by $\sqrt{N/a_{\text{osc}}^3}$. Here, m is the mass of the atoms and N is the total number of atoms in the system, and ω is the trapping frequencies along x and y directions of the harmonic trap. We denote N_1 and N_2 as the number of atoms in condensates Ψ_1 and Ψ_2 respectively, and consider the total number, $N = N_1 + N_2$, is conserved during and after the transfer process. We point out that initially $N_1 = N$ and $N_2 = 0$. Note that, the parameter associated with the peak Rabi frequency, \mathcal{V}_{\max} , contains parameters from the considered atomic transition, laser pulses and the trap of the condensate. The quasi-2D configuration of the trap is achieved by ensuring large trapping frequency in z direction, that is, $\omega_z \gg \omega$. The intra and inter-component coupling strengths are $\mathcal{G}_{ii} = 2N\sqrt{2\pi\lambda}a_{ii}/a_{\text{osc}}$ and $\mathcal{G}_{ij} = \mathcal{G}_{ji} = 2N\sqrt{2\pi\lambda}a_{ij}/a_{\text{osc}}$, respectively, and $\lambda = \omega_z/\omega$ is the anisotropy parameter. The intra-component and inter-component scattering lengths are denoted by a_{ii} and a_{ij} , respectively. Initially, only the condensate Ψ_1 is present within the trap. With two photon Raman transitions, the condensate Ψ_2 grows by gaining atoms from the condensate Ψ_1 . During this process atoms in Ψ_2 gain $(l_1 - l_2)$ unit orbital angular momentum, which is manifested as a phase factor $e^{i(l_1-l_2)\phi}$ in the condensate wavefunction Ψ_2 . The phase factor $e^{-i(l_1-l_2)\phi}$ in the coupling term of Equation (3) ensures that no angular momentum is transferred back to the atoms in condensate Ψ_1 . Transfer of this angular momentum to the condensate Ψ_2 results in generating quantized vortex in the condensate. A quantized vortex in a BEC is point like topological defect which is manifested in the phase profile of the condensate wavefunction Ψ_2 . Around the vortex the phase of the condensate wavefunction changes by $\kappa \times 2\pi$, where κ is an integer, which is referred to as the winding number or charge of the vortex.

A system of two component BECs can exhibit two phases, miscible or immiscible, depending on the the strengths of intracomponent and intercomponent interactions. At zero temperature, two defect free condensates in a homogeneous trap are miscible when $a_{12}^2 \leq a_{11}a_{22}$, and immiscible for $a_{12}^2 \geq a_{11}a_{22}$ [76]. However, these conditions are modified when the condensates are considered in inhomogeneous trap [77]. Effects of finite temperature [70] and topological defects [15] on the miscible-immiscible transition have been reported. A well known measure to characterize these two phases is the overlap integral defined as [15,69,70]

$$\Lambda = \frac{\left[\iint dx dy n_1(x, y) n_2(x, y) \right]^2}{\left[\iint dx dy n_1^2(x, y) \right] \left[\iint dx dy n_2^2(x, y) \right]}, \tag{6}$$

where $n_{1(2)}(x, y) = |\Psi_{1(2)}(x, y)|^2$ are the densities of the condensates. $\Lambda = 0$ corresponds that the two condensates are spatially separated, that is, the system is in immiscible phase. Whereas, $\Lambda = 1$ implies maximal spatial overlap between the condensates, that is, the system is in complete miscible phase.

To this end, by utilizing two-photon Raman transition, we transfer the atoms from one initially populated quantum state to another unpopulated state via an intermediate state, see Figure 1. A pump field links state $|1\rangle$ to electronically excited state $|3\rangle$, and Stokes field links state $|3\rangle$ to another low energy state $|2\rangle$. We perform a one-way controlled particle

transfer from one hyperfine state to another, where atoms of the daughter state carries one unit vorticity, either positive or negative, thus enabling us to create a rotating BEC. In this context, coherent population transfer is possible if the Stokes field precedes, but temporally overlaps with, the pump field, and the pulses are applied adiabatically.

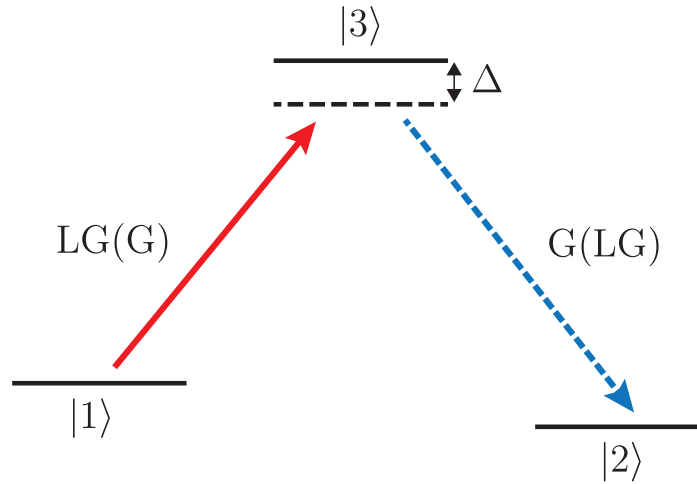


Figure 1. Schematic of the electronic states considered, in a Λ configuration. Specifically, the states of interest are $|1\rangle$ and $|2\rangle$ which represent the states associated with the two-component Bose–Einstein Condensate (BEC). These two states are coupled, via $|3\rangle$, through detuned Gaussian (G) and Laguerre–Gaussian (LG) laser pulses. In this work two laser pulse sequences are considered: (i) G-LG where the Gaussian is the pulse ($|1\rangle \rightarrow |3\rangle$) beam and the Laguerre–Gaussian is the Stokes ($|3\rangle \rightarrow |2\rangle$) beam and (ii) LG-G where the Laguerre–Gaussian is the pulse ($|1\rangle \rightarrow |3\rangle$) beam and the Gaussian is the Stokes ($|3\rangle \rightarrow |2\rangle$) beam.

3. Numerical Methods

We start with a BEC of N atoms at state $|1\rangle$, in the absence of laser pulses. Therefore, we set terms associated with laser pulses in Equation (3) to be zero to obtain the initial solution. Then, the wavefunction of the initial BEC, Ψ_1 , is generated by solving Equation (3) in imaginary time using split-time Crank–Nicolson method [78]. The initial wavefunction of BEC of the atoms in state $|2\rangle$, Ψ_2 , is considered to be zero. Using these two initial wave functions, we evolve the system in presence of laser pulses. For this, we solve the coupled GP equations in Equations (3) and (4) in real time. The phase imprinting in the Ψ_2 occurs dynamically due to the two photon Raman transitions, which is obtained by considering,

$$\Psi_1(x, y, t_{n+1}) = \cos\left(\frac{\mathcal{V}'dt}{2}\right)\Psi_1(x, y, t_n) - ie^{-i(l_1-l_2)\phi} \sin\left(\frac{\mathcal{V}'dt}{2}\right)\Psi_2(x, y, t_n), \quad (7)$$

and

$$\Psi_2(x, y, t_{n+1}) = \cos\left(\frac{\mathcal{V}'dt}{2}\right)\Psi_2(x, y, t_n) - ie^{i(l_1-l_2)\phi} \sin\left(\frac{\mathcal{V}'dt}{2}\right)\Psi_1(x, y, t_n). \quad (8)$$

Since Ψ_2 is zero at the initial time t_0 , $l_1 - l_2$ unit vortex is imprinted on Ψ_2 at $t_1 = t_0 + \delta t$ and vorticity of Ψ_1 remains zero. This transfer of angular momentum continues, as long as both pulses are present. However, since the process is one-way, it stops when all the atoms in condensate Ψ_1 are transferred to the rotating condensate. For simulations, we choose a square grid of 300×300 grid points with a grid spacing $\delta_x = \delta_y = 0.05a_{osc}$ and time step $\Delta t = 0.0001\omega^{-1}$. In our study, we consider hyperfine states of ^{87}Rb with $|1, -1\rangle$ as $|1\rangle$ and $|2, +1\rangle$ as $|2\rangle$. The intracomponent scattering lengths a_{11} and a_{22} of these two states are $100.4a_0$ and $95.44a_0$ [79] respectively, where a_0 is the Bohr radius. The trap frequency $\omega = 2\pi \times 30.832 \text{ Hz}$ [80] and the anisotropy parameter $\lambda = 40$ are the same for both condensates. For this system the oscillator length $a_{osc} = 1.94 \mu\text{m}$. Furthermore, the relation

$\mu_{1(2)} \ll \hbar\omega_z$ holds throughout the time evolution indicating that quasi-2D configuration is maintained always. Total number of atoms in the system is $N = 10^4$. To create a BEC with a vortex of charge -1 unit, we use G pulse as “pump” of which $l_1 = 0$, and LG Pulse as “Stokes” with $l_2 = 1$. If we interchange the “pump” and “Stokes” laser pulses, a vortex of charge $+1$ unit will be created in the BEC. For simulations, we use the pulses with same temporal duration of $T = 4.9$ ms.

4. Results and Discussion

4.1. Creation of Vortex in the BEC

In G-LG pulse sequence, we employ G pulse as pump and LG pulse as Stokes, for which $l_1 = 0$ and $l_2 = 1$ respectively. For this arrangement, we consider $\tau_1 = 1.4$ and $\tau_2 = 1.0$ in the units of $1/\omega$. During the Raman transitions of atoms from state $|1\rangle$ to $|2\rangle$ an amount of -1 unit OAM is transferred to the atoms in state $|2\rangle$. Here, we describe the transfer process. First, a photon from the G laser pulse which has zero OAM is absorbed by the atom in $|1\rangle$. As a result, the atom is excited to an intermediate excited state $|3\rangle$. Then, a photon with $+1$ unit OAM is emitted by the atom at the state $|3\rangle$ onto the LG beam. After this emission process the atom comes back to another ground state $|2\rangle$. The conservation of the total angular momentum of the system, that is, the total angular momentum of atom plus light pulses, ensures that atom at the state $|2\rangle$ gains -1 unit OAM. Thus, -1 unit vorticity is created in the condensate Ψ_2 . Similarly, $+1$ unit vorticity can be created in the condensate Ψ_2 through LG-G pulse sequence, where we use LG pulse as pump and G pulse as Stokes of which $l_1 = 1$ and $l_2 = 0$ respectively.

4.2. Density Evolution of the Condensates

We have discussed that the sign of the vorticity in condensate Ψ_2 depends on the laser modes chosen as pump and Stokes beam. Here, we point out how the sign of the vorticity can be inferred from the changes of density patterns of the condensates during the transfer process. Furthermore, these density patterns serve as promising candidates to elucidate the residual excitations created during the light–matter interaction, since these excitations leave their foot-prints on the density profiles creating additional humps and dips [81,82]. Figure 2(a_1 – a_6, b_1 – b_6) illustrate the density profiles of the condensates during the Raman transitions, when the vortex of charge -1 unit is generated in the condensate Ψ_2 . Whereas, Figure 2(c_1 – c_6, d_1 – d_6) illustrate the density profiles when $+1$ unit vortex is created. In the lower-left corner of each density profile we mention the fraction of atoms in the condensate with respect total number of atoms in the system.

From the comparison between the Figure 2(a_1 – a_6, b_1 – b_6, c_1 – c_6, d_1 – d_6), it is evident that density patterns of the condensates during the creation of -1 unit vortex are different from the case of creation of $+1$ unit vortex. During the initial growth of the condensate Ψ_2 , the atoms occupy the central region of the trap when the vortex of charge -1 unit is created, whereas the atoms occupy the peripheral region of the trap when the $+1$ unit vortex created. At $t = 0$, the laser pulses are absent and the condensate Ψ_1 is populated by all the atoms in the system, hence, the condensate Ψ_2 is empty. It is important to mention that for the coherent population transfer, we apply the Stokes beam first. Therefore, in the early stage of the dynamics population of condensate Ψ_2 remains zero. Once the pump beam is applied, condensate Ψ_2 starts growing at the expense of atoms being transferred from the condensate Ψ_1 . At the same time, a vortex of either -1 or $+1$ unit is imprinted on condensate Ψ_2 depending on the angular momenta of the pump and Stokes beams. For the case of LG-G pulse sequence, which is illustrated in Figure 2(c_1 – c_6, d_1 – d_6), we observe that 11% of atoms has been transferred in the first 10.84 ms, but 68% of atoms are transferred in the next 1.96 ms. In contrast to this, we observe that fewer numbers of atoms are transferred to condensate Ψ_2 at the same time instants when compared to the G-LG pulse sequence, which is also evident from Figure 2(b_1 – b_6). In both the cases, the generated vortex appears with core, that is, zero density region at the center of condensate Ψ_2 , which is visible in the density profiles of Ψ_2 shown in Figure 2(b_1 – b_6, d_1 – d_6). It is worth noting

that density depleted region at the center of the trap is also observed in the density profiles of condensate Ψ_1 during the creation of -1 unit vortex in Ψ_2 (Figure 2(a_1 – a_6)). However, such a hole is absent in the condensate Ψ_1 , when $+1$ unit vortex is created. To understand the nature of the density depleted regions, we study the phase profiles of the condensates. We confirm the presence of phase discontinuity at the center of condensate Ψ_2 for both the cases. It is mentioned earlier that the phase of the condensate wavefunction changes by $\kappa \times 2\pi$ around a quantized vortex, where κ is the winding-number or charge of the vortex. We compute the winding number κ to be -1 when we use G as pulse and LG as Stokes beam, whereas $\kappa = +1$ when we consider LG-G pulse sequence. On the other hand, the phase profile of the condensate Ψ_1 does not possess phase discontinuity during the transfer process for both cases. Thus, the hole in condensate Ψ_1 which is generated during the application of G-LG pulse sequence, is not a vortex.

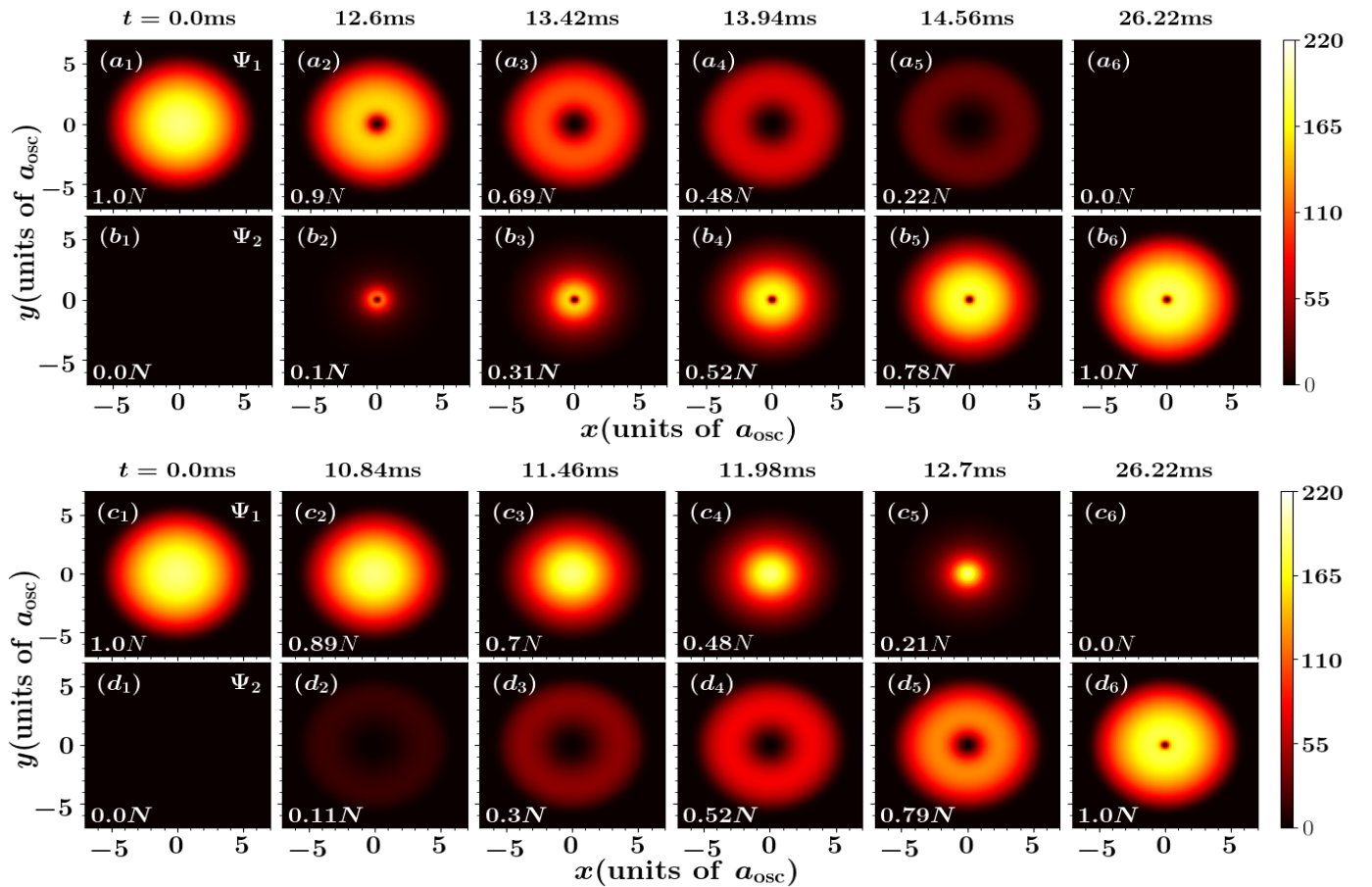


Figure 2. (Color online) Shows the time evolution of density profiles of the condensates of (a_1 – a_6), (c_1 – c_6) atoms in $|1\rangle$ and (b_1 – b_6), (d_1 – d_6) those in $|2\rangle$, when -1 unit [(b_1 – b_6)] and $+1$ [(d_1 – d_6)] unit vortex is created in the condensate Ψ_2 . In the course of time, the condensate Ψ_2 gets populated. The fraction of atoms in the condensate with respect to total number of atoms $N = 10^4$, is mentioned at the bottom left corner of each figure. Atoms are kick-started to be transferred from the condensate Ψ_1 to the condensate Ψ_2 in the central region of the trap for -1 unit vortex transfer, but in the peripheral region of the trap for $+1$ unit vortex transfer. Almost 100% atoms get transferred to state $|2\rangle$ for both the cases.

Focusing our discussion on G-LG pulse sequence, we ascribe the presence of hole in condensate Ψ_1 to the distortion of harmonic trap potential by the optical dipole potential. In this case, the optical dipole potential is induced by the G laser pulse for the condensate Ψ_1 and by the LG laser pulse for the condensate Ψ_2 . Note that, at $t = 0$ ms the laser pulses are absent and the minimum of the harmonic oscillator occurs at the center of the trap. Hence, we obtain a pancake-shaped density profile of the condensate Ψ_1 , which has maximum density at the trap center to minimize trap potential energy. Then, during the application

of laser pulse, the G-pulse gradually creates a rotationally symmetric “hump” at the center of the trap, which increases the potential energy at the trap center. Therefore, the minimum of the effective trap potential $V_{\text{eff},1}$ gets shifted radially away from the center, resulting in a rotationally symmetric annular region as the new minimum of the potential. It is important to mention that the density profile of a condensate in a binary mixture depends on the effective trap potential in conjunction with the number of atoms in the condensate, intra and intercomponent scattering length. Therefore, the atoms of the condensate Ψ_1 move away from center of the trap and settle at the annular region to minimize the trap potential energy. This creates a hole at the center of the density profile of the condensate Ψ_1 . Since the optical dipole potential induced by LG pulse has parabolic form around the center of the trap, the position of the minimum of the effective potential $V_{\text{eff},2}$ does not change over time. However, the steepness of this effective potential changes with time. It increases up to time $t = \tau_1$ and then gradually decreases back to its initial value which is determined by the considered harmonic potential. Therefore, the atoms in the condensate Ψ_2 are always pushed towards the center of the trap to minimize trap potential energy. As a result, during the growth of Ψ_2 , the central region of the trap is occupied by the transferred atoms first, and then rest of the region is occupied.

For LG-G pulse sequence, laser modes of pump and Stokes beam are interchanged. Now the optical dipole potential is induced by the LG laser pulse for the condensate Ψ_1 and by the G laser pulse for the condensate Ψ_2 . Therefore, with the increase of the steepness of the parabolic potential, which is generated by the LG pulse, the atoms in the condensate Ψ_1 are pushed towards the central region of the trap. The atoms that are transferred to condensate Ψ_2 experience the “hump” in the trap potential at the center, which is created by the G pulse. Thus, the atoms in condensate Ψ_2 are pushed towards an annular minimum region of the effective trap potential. This results in larger core of the vortex in condensate Ψ_2 during the transfer process, which is to be contrasted with the previous case.

4.3. Root-Mean-Square Radius of the Condensates

The growth rate of condensate Ψ_2 can be inferred from the rate of change of rms radii of the condensates. In Figure 3 we illustrate the evolution of the r_{rms} of both condensates during the transfer process for the cases when G-LG and LG-G pulse sequences are considered. From the comparison between the considered cases, we can infer that the growth rate of the condensate Ψ_2 is faster in the case of LG-G pulse sequence than the case of G-LG pulse sequence. Note that, for the chosen pulses, the strength of the Raman interaction term \mathcal{V}' is always maximum, at the boundary of the trap. However, atoms in the condensate try to occupy the minimum of the trap potential to minimize the trap potential energy. In particular, the effective trap potential $V_{\text{eff},2}$ of condensate Ψ_2 has a minimum at the center of trap for G-LG pulse sequence, but at a distance $r = w_0 \sqrt{\ln(4\mathcal{V}_2(t)/w_0^2)}/2$ from the center, for LG-G pulse sequence. Therefore, in the later case, the minimum of the effective trap potential is closer to the trap boundary where the Raman coupling \mathcal{V}' term is maximum.

This suggests that the growth rate of the condensate Ψ_2 depends on the distance between the position of the minimum of effective trap potential and the position of maximum Raman coupling. After the transfer process, the rms radius of Ψ_2 oscillates around a mean value. The frequency of such residual radial oscillations, as can be seen from Figure 3, is approximately $\omega' = \omega/3$ for both pulse sequences. The amplitude of oscillation is much smaller than the mean radius of condensate. Most importantly, such a small amplitude of oscillation indicates that negligible amount residual excitations have been activated during the population transfer. However, detail analysis of such excitations is out of the scope of this work.

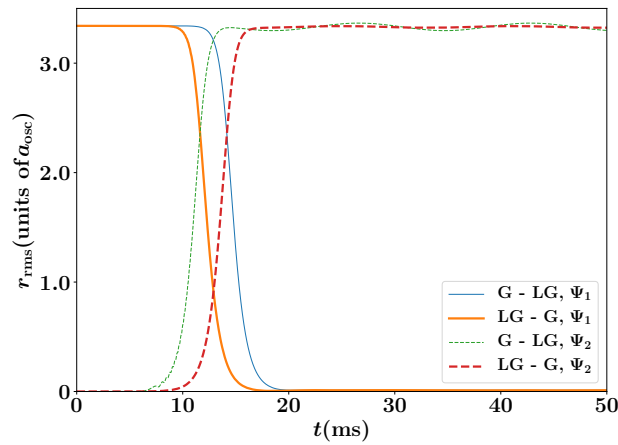


Figure 3. (Color online) Shows the time evolution root mean square radius r_{rms} of BEC Ψ_1 and Ψ_2 for different pulse sequences (see legends). The BECs are confined harmonic trapping potential with frequency $\omega = 2\pi \times 30.832$ Hz and the intra- and interspecies interactions are taken as $a_{11} = 100.04a_0$, $a_{22} = 95.44a_0$, and $a_{12} = 100a_0$ respectively. The dynamics is triggered by employing LG[G]-G[LG] pulse sequence, where LG[G] is the pump beam and G[LG] is the Stokes beam.

4.4. Effects of Intercomponent Interaction

We now discuss the effects of intercomponent interaction between the two condensates, during the transfer process and the final population of the condensate Ψ_2 . We consider the LG-G pulse sequence as the representative example.

The scattering length a_{12} , which quantifies interactions between the atoms of the two different components, plays an important role in determining spatial wavefunctions and the energy of the condensates. Indeed, for certain temporal duration of pulses and intercomponent scattering length, the strength of the atom-light interaction \mathcal{V}_{max} have to be monitored to get the desired population of atoms in the state $|2\rangle$. In the Figure 4, we present the number of atoms in condensate Ψ_2 at the end of the transfer process as a function of a_{12} and \mathcal{V}_{max} . We vary peak Rabi frequency \mathcal{V}_{max} from 1 to 100 and intercomponent atomic scattering length a_{12} from $70a_0$ to $110a_0$. Peak Rabi frequency can be controlled either by changing peak light intensity of the pulse or by changing the detuning. Whereas, the scattering length can be varied through the magnetic Feshbach resonance [83]. We observe complete population transfer from condensate Ψ_1 to condensate Ψ_2 when \mathcal{V}_{max} is greater than 100 (not shown in the diagram). Intercomponent interactions merely affect the transfer process. In this region, atom-light interaction is strong enough to affect any density distribution determined by a_{12} . However, this situation does not hold for intermediate values of \mathcal{V}_{max} , predominantly between 100 and 10. In this region, stronger is the intercomponent interaction, larger is the number of atoms transferred to condensate Ψ_2 . For small values of \mathcal{V}_{max} , larger values of a_{12} suppresses the transfer process, which is evident from Figure 4. It is important to mention that in this limit, we observe the growth of condensate Ψ_2 is different for different values of intercomponent atomic scattering length. That is, depending on the strength of the atom-light interaction, a_{12} affects the population transfer in different manner. For example, for $\mathcal{V}_{\text{max}} = 1$, the final population of Ψ_2 is suppressed for larger a_{12} , whereas, for $\mathcal{V}_{\text{max}} = 10$, strong interaction increases the population in Ψ_2 (see Figure 5a,b).

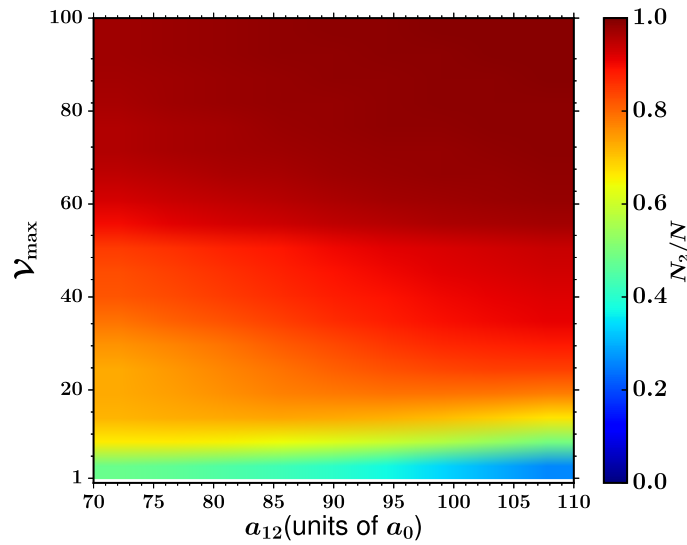


Figure 4. (Color online) Illustrates the number of atoms transferred to the condensate Ψ_2 as a function of intercomponent scattering length a_{12} and the light-matter interaction parameter \mathcal{V}_{\max} . The colorbar shows the fraction of atoms in condensate Ψ_2 with respect to the total number of atoms $N = 10^4$ in the system at the end of the transfer process. The population transfer from Ψ_1 to Ψ_2 is carried-out using LG(pump)-G(stokes) pulse sequence. The system is confined in a harmonic trapping potential with frequency $\omega = 2\pi \times 30.832$ Hz and the intraspecies scattering lengths are $a_{11} = 100.04a_0$ and $a_{22} = 95.44a_0$.

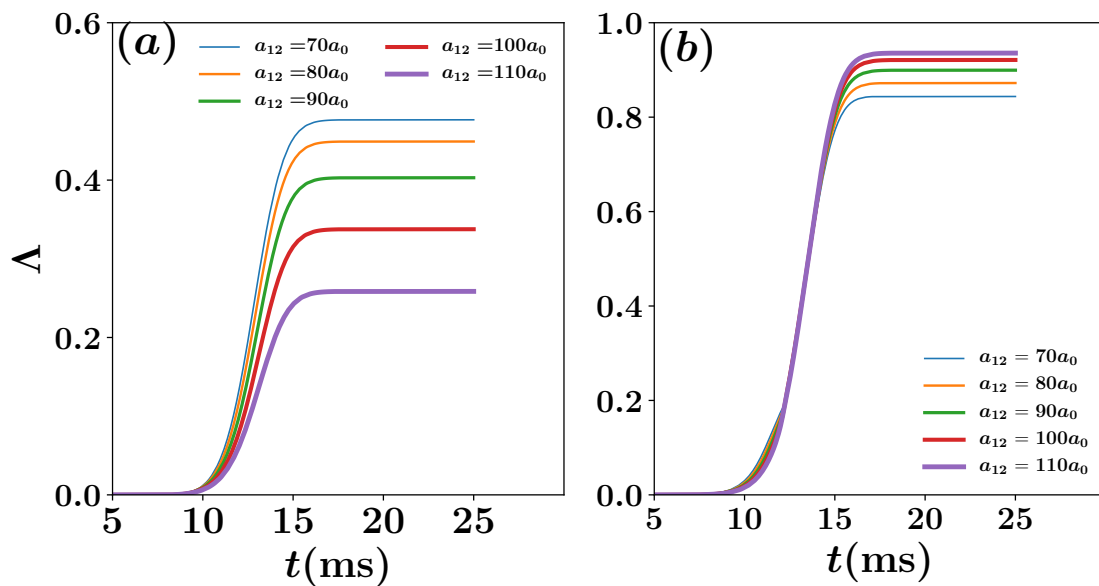


Figure 5. (Color online) Shows the time evolution of the population in the condensate Ψ_2 for a fixed Rabi frequency, with (a) $\mathcal{V}_{\max} = 1$ and (b) $\mathcal{V}_{\max} = 10$, and different interspecies scattering lengths a_{12} [see legends]. The dynamics is triggered by employing LG(pump)-G(stokes) pulse sequence. The BEC Ψ_2 is confined in a harmonic trapping potential with frequency $\omega = 2\pi \times 30.832$ Hz. The total number of atoms in the system is $N = 10^4$ and the intraspecies scattering lengths are given by $a_{11} = 100.04a_0$ and $a_{22} = 95.44a_0$. For $\mathcal{V}_{\max} = 1$, larger a_{12} suppresses the population transfer processes, but favors the same for $\mathcal{V}_{\max} = 10$.

In order to gain further intuition regarding the combined effect of the atom-light coupling and inter-component interaction we resort to the density evolution. Figure 6 presents few representative snapshots of the density profiles for $\mathcal{V}_{\max} = 1$ and $a_{12} = 80a_0$. Note that this particular parameter set corresponds to 45% particle transfer to Ψ_2 (see Figure 5), therefore, enabling the creation of binary mixture of almost equal particles. This, in par-

ticular, is better comprehended from the density profiles depicted in Figure 6. Preparing the initial state characterized by all the atoms residing at the state $|1\rangle$ (Figure 6(a_1, b_1)), the light–matter interaction is initiated by employing LG–and G beams as pump and stokes beam, respectively. Note that the large vortex core of Ψ_2 during the early stage of population transfer is caused by the presence of the Gaussian potential barrier at its center (see Figure 6(b_2)). However, the same vortex core gradually shrinks as more number of particles are transferred and the Gaussian barrier gradually diminishes (see Figure 6(b_3, b_4)). Finally, the BEC at $|2\rangle$ possess 45% of the total number of particles. A close inspection of Figure 6($a_4–a_6, b_4–b_6$) reveals that a breathing motion characterized by expansion and contraction of the density profiles has been triggered in both Ψ_1 and Ψ_2 . Another observation is that Ψ_2 , after the population transfer, exhibits larger vortex core when compared to the case of complete particle transfer, see Figure 2(d_6) and Figure 6(b_6).

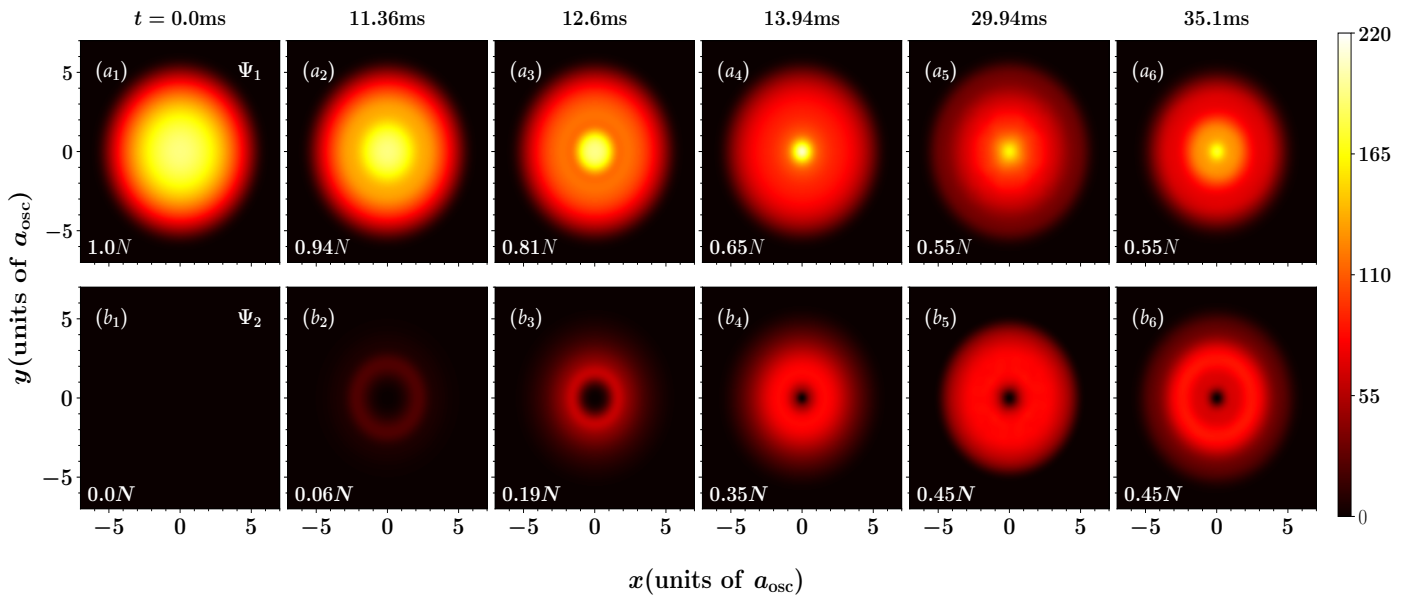


Figure 6. (Color online) Shows the time evolution (see the legends) of the density profiles of the BEC Ψ_1 at ($a_1–a_6$) $|1\rangle$ and those of BEC Ψ_2 at ($b_1–b_6$) $|2\rangle$. The population transfer from Ψ_1 to Ψ_2 is triggered by utilizing a LG(pump)–G(stokes) pulse sequence and setting the light–matter interaction parameter $\mathcal{V}_{\max} = 1$ and the interspecies scattering length $a_{12} = 80a_0$, while all other parameters are the same as before. The fraction of atoms the condensate with respect to the total number of atoms $N = 10^4$, is mentioned at the bottom left corner of each figure.

In addition, we observe the peak Rabi frequency plays an important role in determining the miscibility between the two components during light–matter interaction. This is in contrast to the case when the light field is absent, that is, miscibility of two condensates is determined by the intra and intercomponent interactions. To illustrate this, we have considered Rabi frequencies, $\mathcal{V}_{\max} = 1$ and $\mathcal{V}_{\max} = 10$, for which both the condensates Ψ_1 and Ψ_2 have finite number of atoms N_1 and N_2 , even after the light–matter interaction. For these two cases, we show the variation of the miscibility parameter Λ with time in Figure 7. Note that just after the initiation of the transfer process, condensate Ψ_2 grows within the condensate Ψ_1 , resulting in gradual increase of Λ . However, when a sufficient number of atoms have been transferred to condensate Ψ_2 and both the pulses have significant temporal overlap, mutual repulsion between the condensates and the optical dipole potential tend to push the two condensates away from each other. This results in decrease of Λ . Again, the overlap between the condensates and hence Λ increases as pulses gradually die down. It is important to notice that during the light–matter interaction we obtain larger values of Λ for larger values of a_{12} . This indicates, the stronger the intercomponent repulsion between the two condensates, the larger the overlap between them is. This is to be contrasted with the case when light–matter interaction is absent, in which, larger intercomponent repulsion

separates the condensates spatially. After the light–matter interaction, that is, when the optical dipole potentials disappear, the miscibility between the condensates is determined by intra- and inter-component interactions.

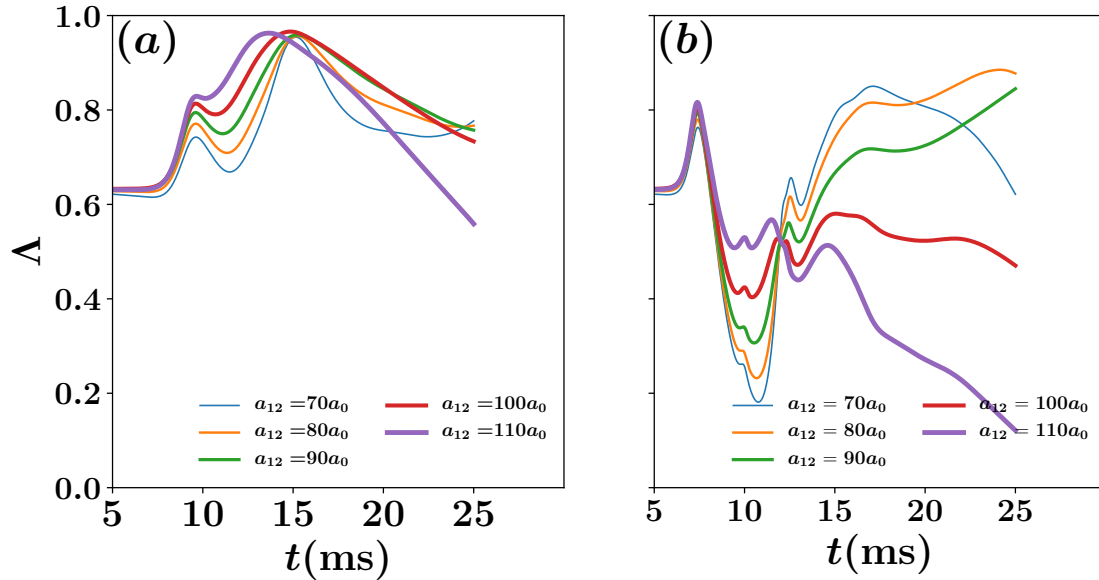


Figure 7. (Color online) Shows the time evolution of the overlap integral Δ for a fixed Rabi frequency, with (a) $\mathcal{V}_{\max} = 1$ and (b) $\mathcal{V}_{\max} = 10$, and different interspecies scattering lengths a_{12} [see legends]. The dynamics is initiated by employing LG(pump)-G(stokes) pulse sequence. The binary BECs are confined in harmonic trapping potential with frequency $\omega = 2\pi \times 30.832$ Hz. The total number of atoms in the system is $N = 10^4$ and the intraspecies scattering lengths are given by $a_{11} = 100.04a_0$ and $a_{22} = 95.44a_0$.

5. Conclusions

In conclusion, we have shown that how two-photon Raman transition can be used to generate a rotating BEC with vorticity of either sign, by transferring atoms from another condensate. In this transition, atoms gain angular momentum from the LG laser pulse before being transferred to a rotating condensate. Density patterns of the condensates during the light–matter interaction depend on sign of the vorticity of the rotating condensate.

In particular, we have show that how a specific choice of pump and stokes beams can alter the locations, within the trap, where the transferred particles start accumulating. Notably, this result stems form the optical potentials felt by the atoms of each individual state. Most importantly, the interchange of pump and stokes laser beams not only changes the sign of vorticity, but also gives rise different dipole potentials influencing both the growth rate and growth region of the new Bose–Einstein condensate. The growth of the new condensate with -1 unit vorticity is started from the central region of the trap, but a condensate with $+1$ unit vorticity starts to grow from the peripheral region of the same. Furthermore, the “smoothness” of the density profiles and the temporal evolution of rms radius imply that there are very few excitations emerging during the light–matter interaction.

Moreover, we have shown that the number of transferred atoms can be monitored by tuning the intercomponent interaction, if the peak Rabi frequency of light–matter interaction is low and in particular, large intercomponent interaction subdues this transfer process. In this way, by maneuvering the atom–light interaction strength and the intercomponent scattering length one can create binary mixture of condensates.

Another major finding from our investigation is that intercomponent interaction kind of plays an opposite role in the process of phase separation during the Raman transition process, in contrast to literature [84] when such dynamical perturbation is absent. We find that a stronger intercomponent interaction favors greater miscibility between the condensates during the light–matter interaction.

Finally, we point out that the storage of a photon pair entangled in OAM space through Raman transition in the cold atomic ensemble has served as a sandbox to study information processing [85]. Besides, because atoms can have higher spin manifolds than light, the extension of our work to the spinor BEC would be an important study. Various topological properties can be developed in the ground state depending on Rabi frequency and atom-atom interaction strength, for example, a Mermin-Ho vortex or a meron pair phase [86], and might lead to the exhibition of non-Abelian braiding statistics [87] which is particularly interesting for topological quantum computing protocols [88]. We expect our study will shed light for further research in this direction.

Author Contributions: Conceptualization, K.M., A.M.M. and S.M.; methodology, K.M., S.B. and D.A.; software, K.M. and S.B.; validation, K.M.; formal analysis, K.M.; investigation, K.M.; resources, S.M.; data curation, K.M.; writing—original draft preparation, K.M.; writing—review and editing, K.M., S.B., D.A., A.M.M. and S.M.; visualization, K.M.; supervision, S.M.; project administration, S.M.; funding acquisition, K.M. and S.M. All authors have read and agreed to the published version of the manuscript.

Funding: K.M. acknowledges MHRD, Govt of India for the research fellowship.

Institutional Review Board Statement: Not applicable.

Informed Consent Statement: Not applicable.

Data Availability Statement: All the data that support the plots within this paper are available from the corresponding author upon reasonable request.

Acknowledgments: K.M. is thankful to Subrata Das for technical assistance. K.M. is also grateful to Physical Research Laboratory, Ahmedabad for the hospitality during the initial stages of this work. S.B. and D.A. gratefully thank Arko Roy and Pekko Kuopanportti for insightful discussions.

Conflicts of Interest: The authors declare no conflict of interest. The funders had no role in the design of the study; in the collection, analyses, or interpretation of data; in the writing of the manuscript, or in the decision to publish the results.

Appendix A. Effects of Harmonic Trap and Time-Delay between the Pulses

Here we discuss the effects of the trapping frequencies of the harmonic potentials and the time-delay between two pulses during the particle transfer and on the final population of the component Ψ_2 . In particular, we are interested in the weak atom-light coupling regime where both components contain finite number of particles. To that purpose we set $\mathcal{V}_{\max} = 1$, also the interspecies scattering length is $a_{12} = 80a_0$. Figure A1a presents time evolution of the fraction of total number of particles in Ψ_2 for different trapping frequencies ω . It is evident that consideration of a different trapping frequency only changes the time scale of the relevant phenomenology. Remarkably, it does not alter the final population of the Ψ_2 to a great extent. The onset and the growth rate of the population transfer are influenced by the trapping frequency. For instance, for $\omega/(2\pi) = 30.832$ Hz, the transfer starts at earlier time instant and occurs at a faster rate when compared to the others.

Next we inspect the effect of varying time-delay between the two pulses on the population transfer in the weak light-matter coupling regime (see Figure A1b). We fix the peak location (τ_2) of the Stokes pulse at $\tau_2 = 10.33$ ms and vary the peak location (τ_1) of the pump pulse. We notice that maximum particle transfer is approximately 45% of the total population, which is achieved when τ_1 lies in the range 11.36–12.39 ms. However, when the time delay is too large ($\tau_1 = 15.49$ ms) or too small ($\tau_1 = 10.36$ ms) the number of particles in Ψ_2 decreases. Besides, when the time delay is very small, in other words temporal peaks of the two pulses are very close to each other, the growth of the population shows a very different behavior, see the blue curve in Figure A1b. The noticeable swell, during the light-matter interaction, in the curve corresponding to $\tau_1 = 10.36$ ms can be related to the creation of significant amount of excitations in both components. These excitations stemming from the interactions with laser pulses also remain in both components after the interaction is over. We remark that such residual excitations leave their finger-prints

onto the density profiles of the components (not shown here for the brevity), and bear the signatures of the break-down of coherent population transfer.

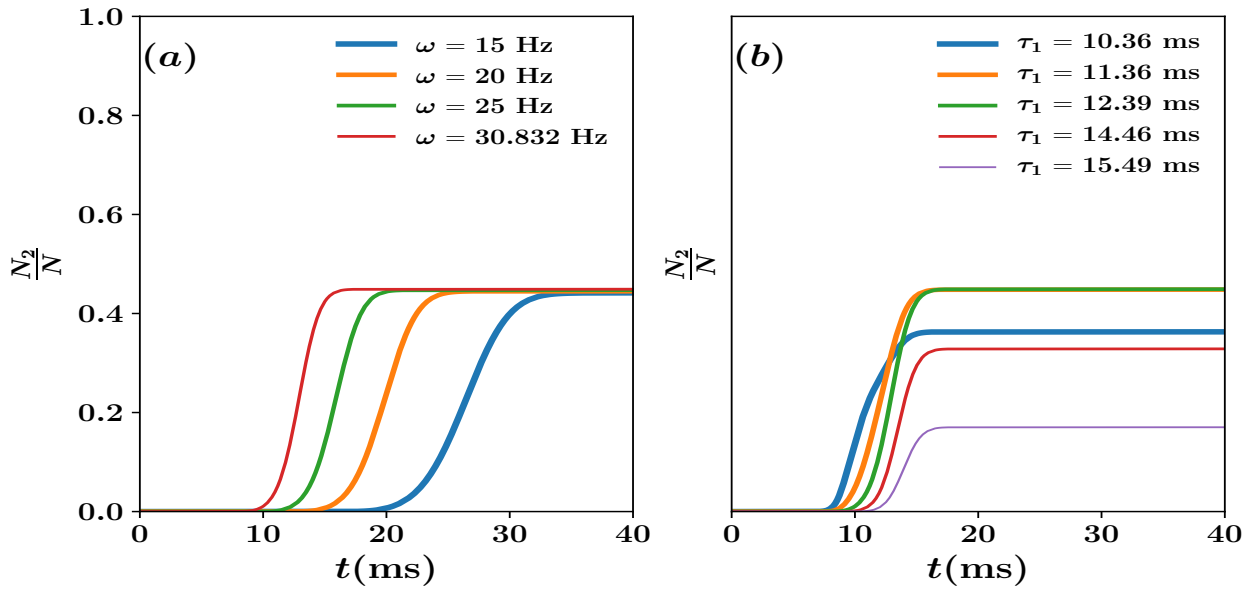


Figure A1. (Color online) Time evolution of the fraction of particle number transferred to the BEC Ψ_2 for (a) various trapping frequencies ω and (b) various peak positions of the (τ_1) of the pump laser pulse. A LG-G pulse sequence is used to trigger the dynamics in the weak light–matter interaction regime characterized by $\mathcal{V}_{\max} = 1$. While studying the effect of the trapping frequencies [(a)], τ_2 and τ_1 are fixed at 10.33 ms and 13.43 ms, respectively. On the other, the rapping frequency $\omega = 2\pi \times 30.832$ Hz and peak position $\tau_2 = 10.33$ of stokes pulse are kept fixed when studying the variation of τ_1 [(b)]. The total number of particles in the system is $N = 10^4$, and the intra-and interspecies interactions are $a_{11} = 99a_0$, $a_{22} = 95.44a_0$ and $a_{12} = 80a_0$.

Appendix B. Hamiltonian and Derivation of Equation of Motions

Let $\hat{\Psi}_j^\dagger$ and $\hat{\Psi}_j$ be the creation and annihilation operators respectively for atoms at state $|j\rangle$. The Hamiltonian for interacting boson alkali atoms in a trap potential, with respect to a frame rotating at the frequency of applied laser fields in the rotating wave approximation can be written as

$$\begin{aligned}
 H = & \int d\mathbf{r}_1 \hat{\Psi}_1^\dagger(\mathbf{r}_1, t) \hat{h}_1 \hat{\Psi}_1(\mathbf{r}_1, t) + \int d\mathbf{r}_2 \hat{\Psi}_2^\dagger(\mathbf{r}_2, t) \hat{h}_2 \hat{\Psi}_2(\mathbf{r}_2, t) + \hbar\Delta \int d\mathbf{r}_3 \hat{\Psi}_3^\dagger(\mathbf{r}_3, t) \hat{\Psi}_3(\mathbf{r}_3, t) \\
 & + \frac{U_{11}}{2} \int d\mathbf{r}_1 \hat{\Psi}_1^\dagger(\mathbf{r}_1, t) \hat{\Psi}_1^\dagger(\mathbf{r}_1, t) \hat{\Psi}_1(\mathbf{r}_1, t) \hat{\Psi}_1(\mathbf{r}_1, t) + \frac{U_{22}}{2} \int d\mathbf{r}_2 \hat{\Psi}_2^\dagger(\mathbf{r}_2, t) \hat{\Psi}_2^\dagger(\mathbf{r}_2, t) \hat{\Psi}_2(\mathbf{r}_2, t) \hat{\Psi}_2(\mathbf{r}_2, t) \\
 & + U_{12} \int d\mathbf{r}' \hat{\Psi}_1^\dagger(\mathbf{r}', t) \hat{\Psi}_2^\dagger(\mathbf{r}', t) \hat{\Psi}_1(\mathbf{r}', t) \hat{\Psi}_2(\mathbf{r}', t) + \hbar \int d\mathbf{r}' \Omega_1(\mathbf{r}', t) e^{i\phi} \hat{\Psi}_3^\dagger(\mathbf{r}', t) \hat{\Psi}_1(\mathbf{r}', t) \\
 & + \hbar \int d\mathbf{r}' \Omega_2(\mathbf{r}', t) e^{i\phi} \hat{\Psi}_3^\dagger(\mathbf{r}', t) \hat{\Psi}_2(\mathbf{r}', t) + H.c
 \end{aligned}$$

we have following commutation relations for the bosonic operators:

$$\begin{aligned}
 [\hat{\Psi}_j(\mathbf{r}, t), \hat{\Psi}_k^\dagger(\mathbf{r}', t)] &= \delta(\mathbf{r} - \mathbf{r}') \delta_{jk}, \\
 [\hat{\Psi}_j(\mathbf{r}, t), \hat{\Psi}_k(\mathbf{r}', t)] &= 0, \\
 [\hat{\Psi}_j^\dagger(\mathbf{r}, t), \hat{\Psi}_k^\dagger(\mathbf{r}', t)] &= 0
 \end{aligned} \tag{A1}$$

Now Heisenberg equation of motion gives

$$i\hbar \frac{\partial \hat{\Psi}_1(\mathbf{r}, t)}{\partial t} = [\hat{\Psi}_1(\mathbf{r}, t), H] \tag{A2}$$

$$i\hbar \frac{\partial \hat{\Psi}_2(\mathbf{r}, t)}{\partial t} = [\hat{\Psi}_2(\mathbf{r}, t), H] \tag{A3}$$

$$i\hbar \frac{\partial \hat{\Psi}_3(\mathbf{r}, t)}{\partial t} = [\hat{\Psi}_3(\mathbf{r}, t), H] \tag{A4}$$

Using bosonic commutation relation and Heisenberg equation of motion we get

$$i\hbar \frac{\partial \hat{\Psi}_1(\mathbf{r}, t)}{\partial t} = \hat{h}_1 \hat{\Psi}_1(\mathbf{r}, t) + U_{11} \hat{\Psi}_1^\dagger(\mathbf{r}, t) \hat{\Psi}_1(\mathbf{r}, t) \hat{\Psi}_1(\mathbf{r}, t) + U_{12} \hat{\Psi}_2^\dagger(\mathbf{r}, t) \hat{\Psi}_2(\mathbf{r}, t) \hat{\Psi}_1(\mathbf{r}, t) + \Omega_1^*(\mathbf{r}, t) e^{-i l_1 \phi} \hat{\Psi}_3(\mathbf{r}, t), \tag{A5}$$

$$i\hbar \frac{\partial \hat{\Psi}_2(\mathbf{r}, t)}{\partial t} = \hat{h}_2 \hat{\Psi}_2(\mathbf{r}, t) + U_{22} \hat{\Psi}_2^\dagger(\mathbf{r}, t) \hat{\Psi}_2(\mathbf{r}, t) \hat{\Psi}_2(\mathbf{r}, t) + U_{21} \hat{\Psi}_1^\dagger(\mathbf{r}, t) \hat{\Psi}_1(\mathbf{r}, t) \hat{\Psi}_2(\mathbf{r}, t) + \hbar \Omega_1^*(\mathbf{r}, t) e^{-i l_2 \phi} \hat{\Psi}_3(\mathbf{r}, t), \tag{A6}$$

and

$$i\hbar \frac{\partial \hat{\Psi}_3(\mathbf{r}, t)}{\partial t} = \hbar \Delta \hat{\Psi}_3(\mathbf{r}, t) + \hbar \Omega_1(\mathbf{r}, t) e^{i l_1 \phi} \hat{\Psi}_1(\mathbf{r}, t) + \hbar \Omega_2(\mathbf{r}, t) e^{i l_2 \phi} \hat{\Psi}_2(\mathbf{r}, t). \tag{A7}$$

Eliminating of the field operator $\hat{\Psi}_3(r, t)$ adiabatically,

$$i\hbar \frac{\partial \hat{\Psi}_3(\mathbf{r}, t)}{\partial t} = 0 \tag{A8}$$

$$\hat{\Psi}_3(\mathbf{r}, t) = -(\Omega_1(\mathbf{r}, t) e^{i l_1 \phi} \hat{\Psi}_1(\mathbf{r}, t) + \Omega_2(\mathbf{r}, t) e^{i l_2 \phi} \hat{\Psi}_2(\mathbf{r}, t)) / \Delta \tag{A9}$$

Putting (A9) into (A5) and (A6) we get,

$$i\hbar \frac{\partial \hat{\Psi}_1(\mathbf{r}, t)}{\partial t} = \hat{h}_1 \hat{\Psi}_1(\mathbf{r}, t) + U_{11} \hat{\Psi}_1^\dagger(\mathbf{r}, t) \hat{\Psi}_1(\mathbf{r}, t) \hat{\Psi}_1(\mathbf{r}, t) + U_{12} \hat{\Psi}_2^\dagger(\mathbf{r}, t) \hat{\Psi}_2(\mathbf{r}, t) \hat{\Psi}_1(\mathbf{r}, t) - \frac{\hbar |\Omega_1(\mathbf{r}, t)|^2}{\Delta} \hat{\Psi}_1(\mathbf{r}, t) - \frac{\hbar \Omega_2(\mathbf{r}, t) \Omega_1^*(\mathbf{r}, t)}{\Delta} \hat{\Psi}_2(\mathbf{r}, t) e^{-i(l_1 - l_2)\phi} \tag{A10}$$

and

$$i\hbar \frac{\partial \hat{\Psi}_2(\mathbf{r}, t)}{\partial t} = \hat{h}_2 \hat{\Psi}_2(\mathbf{r}, t) + U_{22} \hat{\Psi}_2^\dagger(\mathbf{r}, t) \hat{\Psi}_2(\mathbf{r}, t) \hat{\Psi}_2(\mathbf{r}, t) + U_{21} \hat{\Psi}_1^\dagger(\mathbf{r}, t) \hat{\Psi}_1(\mathbf{r}, t) \hat{\Psi}_2(\mathbf{r}, t) - \frac{\hbar |\Omega_2(\mathbf{r}, t)|^2}{\Delta} \hat{\Psi}_2(\mathbf{r}, t) - \frac{\hbar \Omega_1(\mathbf{r}, t) \Omega_2^*(\mathbf{r}, t)}{\Delta} \hat{\Psi}_1(\mathbf{r}, t) e^{i(l_1 - l_2)\phi} \tag{A11}$$

where $\Omega_1(r)$ and $\Omega_2(r)$, Rabi frequencies of the transitions $|1\rangle \rightarrow |3\rangle$ and $|3\rangle \rightarrow |2\rangle$, are given by $\mathbf{E}_1(\mathbf{r}, t) \cdot \mathbf{d}_{13} / \hbar$ and $\mathbf{E}_2(\mathbf{r}, t) \cdot \mathbf{d}_{32} / \hbar$ with d_{13} and d_{32} being the corresponding transition dipole moments. we consider $d_{13} = d_{23} = d$. At $T = 0$, in limit of low energy s -wave scattering, and neglecting quantum fluctuation, the field operator $\hat{\Psi}_j$ can be replaced by a complex valued wavefunction Ψ_j . Therefore, (A3) and (A4) become

$$i\hbar \frac{\partial \Psi_1(\mathbf{r}, t)}{\partial t} = \left[-\frac{\hbar^2}{2m} \nabla^2 + V(\mathbf{r}) - \frac{\hbar |\Omega_1(\mathbf{r}, t)|^2}{\Delta} \right] \Psi_1 + U_{11} |\Psi_1|^2 \Psi_1 + U_{12} |\Psi_2|^2 \Psi_1 - \frac{\hbar \Omega_2(\mathbf{r}, t) \Omega_1^*(\mathbf{r}, t)}{\Delta} \Psi_2(\mathbf{r}, t) e^{-i(l_1 - l_2)\phi} \quad (\text{A12})$$

and

$$i\hbar \frac{\partial \Psi_2(\mathbf{r}, t)}{\partial t} = \left[-\frac{\hbar^2}{2m} \nabla^2 + V(\mathbf{r}) - \frac{\hbar |\Omega_2(\mathbf{r}, t)|^2}{\Delta} \right] \Psi_2 + U_{11} |\Psi_2|^2 \Psi_2 + U_{12} |\Psi_1|^2 \Psi_2 - \frac{\hbar \Omega_1(\mathbf{r}, t) \Omega_2^*(\mathbf{r}, t)}{\Delta} \Psi_2(\mathbf{r}, t) e^{i(l_1 - l_2)\phi} \quad (\text{A13})$$

Using (1) and (4)

$$|\Omega_{(1)2}|^2 = \left(\frac{\mathcal{E}_{max} d_{32}}{\hbar \Delta} \right)^2 e^{-(\frac{t-\tau_1}{T})^2} (x^2 + y^2)^{|l_1(2)|} e^{-2\left(\frac{x^2+y^2}{w_1^2(2)}\right)} \quad (\text{A14})$$

and

$$\Omega_2^* \Omega_1 = \left(\frac{\mathcal{E}_{max} d_{32}}{\hbar \Delta} \right)^2 e^{-(\frac{t-\tau_1}{T})^2 - (\frac{t-\tau_2}{T})^2} (x^2 + y^2)^{\frac{|l_1|+|l_2|}{2}} e^{-\frac{2(x^2+y^2)}{\left(\frac{1}{w_1^2} + \frac{1}{w_2^2}\right)}} \quad (\text{A15})$$

Here the BEC is considered to be confined at $z = 0$ plane and $\omega_1 \approx \omega_2$.

References

1. Rokhsar, D.S. Vortex Stability and Persistent Currents in Trapped Bose Gases. *Phys. Rev. Lett.* **1997**, *79*, 2164. [\[CrossRef\]](#)
2. Mueller, E.; Goldbart, P.M.; Lyanda-Geller, Y. Multiply connected Bose-Einstein-condensed alkali-metal gases: Current-carrying states and their decay. *Phys. Rev. A* **1998**, *57*, R1505(R). [\[CrossRef\]](#)
3. Onofrio, R.; Raman, C.; Abo-Shaeer, J.; Chikkatur, A.; Ketterle, W. Observation of Superfluid Flow in a Bose-Einstein Condensed Gass and their decay. *Phys. Rev. Lett.* **2000**, *85*, 2228. [\[CrossRef\]](#)
4. Kobayashi, M.; Tsubota, M. Quantum turbulence in a trapped Bose-Einstein condensate. *Phys. Rev. A* **2007**, *76*, 045603. [\[CrossRef\]](#)
5. White, A.C.; Proukakis, N.P.; Youd, A.J.; Wacks, D.H.; Baggaley, A.W.; Barenghi, C.F. Turbulence in a Bose-Einstein condensate. *J. Phys. Conf. Ser.* **2011**, *318*, 062003. [\[CrossRef\]](#)
6. Neely, T.W.; Bradley, A.S.; Samson, E.C.; Rooney, S.J.; Wright, E.M.; Law, K.J.H.; Carretero-González, R.; Kevrekidis, P.G.; Davis, M.J.; Anderson, B.P. Characteristics of Two-Dimensional Quantum Turbulence in a Compressible Superfluid. *Phys. Rev. Lett.* **2013**, *111*, 235301. [\[CrossRef\]](#)
7. Barenghi, C.F.; Skrbek, L.; Sreenivasan, K.R. Introduction to quantum turbulence. *Proc. Natl. Acad. Sci. USA* **2014**, *111*, 4647–4652. [\[CrossRef\]](#)
8. White, A.C.; Anderson, B.P.; Bagnato, V.S. Vortices and turbulence in trapped atomic condensates. *Proc. Natl. Acad. Sci. USA* **2014**, *111*, 4719–4726. [\[CrossRef\]](#)
9. Kwon, W.J.; Moon, G.; Choi, J.Y.; Seo, S.W.; Shin, Y.I. Relaxation of superfluid turbulence in highly oblate Bose-Einstein condensates. *Phys. Rev. A* **2014**, *90*, 063627. [\[CrossRef\]](#)
10. Seo, S.W.; Ko, B.; Kim, J.H.; Shin, Y. Observation of vortex-antivortex pairing in decaying 2D turbulence of a superfluid gas. *Sci. Rep.* **2017**, *7*, 4587. [\[CrossRef\]](#)
11. Fedichev, P.O.; Shlyapnikov, G.V. Dissipative dynamics of a vortex state in a trapped Bose-condensed gas. *Phys. Rev. A* **1999**, *60*, R1779–R1782. [\[CrossRef\]](#)
12. Fetter, A.L.; Svidzinsky, A.A. Vortices in a trapped dilute Bose-Einstein condensate. *J. Phys. Condens. Matter* **2001**, *13*, R135. [\[CrossRef\]](#)
13. Koens, L.; Martin, A.M. Perturbative behavior of a vortex in a trapped Bose-Einstein condensate. *Phys. Rev. A* **2012**, *86*, 013605. [\[CrossRef\]](#)
14. Kevrekidis, P.G.; Wang, W.; Carretero-González, R.; Frantzeskakis, D.J.; Xie, S. Vortex precession dynamics in general radially symmetric potential traps in two-dimensional atomic Bose-Einstein condensates. *Phys. Rev. A* **2017**, *96*, 043612. [\[CrossRef\]](#)
15. Bandyopadhyay, S.; Roy, A.; Angom, D. Dynamics of phase separation in two-species Bose-Einstein condensates with vortices. *Phys. Rev. A* **2017**, *96*, 043603. [\[CrossRef\]](#)

16. Mukherjee, K.; Mukherjee, K.; Mistakidis, S.; Kevrekidis, P.G.; Schmelcher, P. Quench induced vortex-bright-soliton formation in binary Bose-Einstein condensates. *J. Phys. B At. Mol. Opt. Phys.* **2020**. [[CrossRef](#)]
17. Isoshima, T.; Machida, K. Vortex stabilization in Bose-Einstein condensate of alkali-metal atom gas. *Phys. Rev. A* **1999**, *59*, 2203–2212. [[CrossRef](#)]
18. Virtanen, S.M.M.; Salomaa, M.M. Effect of the thermal gas component on the stability of vortices in trapped Bose-Einstein condensates. *J. Phys. B At. Mol. Opt. Phys.* **2002**, *35*, 3967. [[CrossRef](#)]
19. García-Ripoll, J.J.; Pérez-García, V.M. Stable and Unstable Vortices in Multicomponent Bose-Einstein Condensates. *Phys. Rev. Lett.* **2000**, *84*, 4264–4267. [[CrossRef](#)]
20. Coddington, I.; Haljan, P.C.; Engels, P.; Schweikhard, V.; Tung, S.; Cornell, E.A. Experimental studies of equilibrium vortex properties in a Bose-condensed gas. *Phys. Rev. A* **2004**, *70*, 063607. [[CrossRef](#)]
21. Shin, Y.; Saba, M.; Vengalattore, M.; Pasquini, T.A.; Sanner, C.; Leanhardt, A.E.; Prentiss, M.; Pritchard, D.E.; Ketterle, W. Dynamical Instability of a Doubly Quantized Vortex in a Bose-Einstein Condensate. *Phys. Rev. Lett.* **2004**, *93*, 160406. [[CrossRef](#)]
22. Isoshima, T.; Okano, M.; Yasuda, H.; Kasa, K.; Huhtamäki, J.A.M.; Kumakura, M.; Takahashi, Y. Spontaneous Splitting of a Quadruply Charged Vortex. *Phys. Rev. Lett.* **2007**, *99*, 200403. [[CrossRef](#)]
23. Kuopanportti, P.; Lundh, E.; Huhtamäki, J.A.M.; Pietilä, V.; Möttönen, M. Core sizes and dynamical instabilities of giant vortices in dilute Bose-Einstein condensates. *Phys. Rev. A* **2010**, *81*, 023603. [[CrossRef](#)]
24. Kuopanportti, P.; Möttönen, M. Splitting dynamics of giant vortices in dilute Bose-Einstein condensates. *Phys. Rev. A* **2010**, *81*, 033627. [[CrossRef](#)]
25. Dodd, R.J.; Burnett, K.; Edwards, M.; Clark, C.W. Excitation spectroscopy of vortex states in dilute Bose-Einstein condensed gases. *Phys. Rev. A* **1997**, *56*, 587–590. [[CrossRef](#)]
26. Choi, S.; Baksmaty, L.O.; Woo, S.J.; Bigelow, N.P. Excitation spectrum of vortex lattices in rotating Bose-Einstein condensates. *Phys. Rev. A* **2003**, *68*, 031605. [[CrossRef](#)]
27. Skryabin, D.V. Instabilities of vortices in a binary mixture of trapped Bose-Einstein condensates: Role of collective excitations with positive and negative energies. *Phys. Rev. A* **2000**, *63*, 013602. [[CrossRef](#)]
28. Middelkamp, S.; Kevrekidis, P.G.; Frantzeskakis, D.J.; Carretero-González, R.; Schmelcher, P. Bifurcations, stability, and dynamics of multiple matter-wave vortex states. *Phys. Rev. A* **2010**, *82*, 013646. [[CrossRef](#)]
29. Kuopanportti, P.; Bandyopadhyay, S.; Roy, A.; Angom, D. Splitting of singly and doubly quantized composite vortices in two-component Bose-Einstein condensates. *arXiv* **2018**, arXiv:1808.08223.
30. Mateo, A.M.N.; Delgado, V. Dynamical Evolution of a Doubly Quantized Vortex Imprinted in a Bose-Einstein Condensate. *Phys. Rev. Lett.* **2006**, *97*, 180409. [[CrossRef](#)]
31. Neely, T.W.; Samson, E.C.; Bradley, A.S.; Davis, M.J.; Anderson, B.P. Observation of Vortex Dipoles in an Oblate Bose-Einstein Condensate. *Phys. Rev. Lett.* **2010**, *104*, 160401. [[CrossRef](#)]
32. Bolda, E.L.; Walls, D.F. Detection of Vorticity in Bose-Einstein Condensed Gases by Matter-Wave Interference. *Phys. Rev. Lett.* **1998**, *81*, 5477–5480. [[CrossRef](#)]
33. Chevy, F.; Madison, K.W.; Bretin, V.; Dalibard, J. Interferometric detection of a single vortex in a dilute Bose-Einstein condensate. *Phys. Rev. A* **2001**, *64*, 031601. [[CrossRef](#)]
34. Freilich, D.V.; Bianchi, D.M.; Kaufman, A.M.; Langin, T.K.; Hall, D.S. Real-Time Dynamics of Single Vortex Lines and Vortex Dipoles in a Bose-Einstein Condensate. *Science* **2010**, *329*, 1182–1185. [[CrossRef](#)]
35. Navarro, R.; Carretero-González, R.; Torres, P.J.; Kevrekidis, P.G.; Frantzeskakis, D.J.; Ray, M.W.; Altıntaş, E.; Hall, D.S. Dynamics of a Few Corotating Vortices in Bose-Einstein Condensates. *Phys. Rev. Lett.* **2013**, *110*, 225301. [[CrossRef](#)]
36. Wilson, K.E.; Newman, Z.L.; Lowney, J.D.; Anderson, B.P. In situ imaging of vortices in Bose-Einstein condensates. *Phys. Rev. A* **2015**, *91*, 023621. [[CrossRef](#)]
37. Marzlin, K.P.; Zhang, W.; Wright, E.M. Vortex Coupler for Atomic Bose-Einstein Condensates. *Phys. Rev. Lett.* **1997**, *79*, 4728–4731. [[CrossRef](#)]
38. Dum, R.; Cirac, J.I.; Lewenstein, M.; Zoller, P. Creation of Dark Solitons and Vortices in Bose-Einstein Condensates. *Phys. Rev. Lett.* **1998**, *80*, 2972–2975. [[CrossRef](#)]
39. Jackson, B.; McCann, J.F.; Adams, C.S. Vortex Formation in Dilute Inhomogeneous Bose-Einstein Condensates. *Phys. Rev. Lett.* **1998**, *80*, 3903–3906. [[CrossRef](#)]
40. Dobrek, L.; Gajda, M.; Lewenstein, M.; Sengstock, K.; Birkl, G.; Ertmer, W. Optical generation of vortices in trapped Bose-Einstein condensates. *Phys. Rev. A* **1999**, *60*, R3381–R3384. [[CrossRef](#)]
41. Petrosyan, K.G.; You, L. Topological phases and circulating states of Bose-Einstein condensates. *Phys. Rev. A* **1999**, *59*, 639–642. [[CrossRef](#)]
42. Ruostekoski, J. Topological phase preparation in a pair of atomic Bose-Einstein condensates. *Phys. Rev. A* **2000**, *61*, 041603. [[CrossRef](#)]
43. Damski, B.; Sacha, K.; Zakrzewski, J. Stirring a Bose-Einstein condensate. *J. Phys. B At. Mol. Opt. Phys.* **2002**, *35*, 4051. [[CrossRef](#)]
44. Shibayama, H.; Yasaku, Y.; Kuwamoto, T. Vortex nucleation in Bose-Einstein condensates confined in a QUIC trap by topological phase imprinting. *J. Phys. B At. Mol. Opt. Phys.* **2011**, *44*, 075302. [[CrossRef](#)]
45. Matthews, M.R.; Anderson, B.P.; Haljan, P.C.; Hall, D.S.; Wieman, C.E.; Cornell, E.A. Vortices in a Bose-Einstein Condensate. *Phys. Rev. Lett.* **1999**, *83*, 2498–2501. [[CrossRef](#)]

46. Madison, K.W.; Chevy, F.; Wohlleben, W.; Dalibard, J. Vortex Formation in a Stirred Bose-Einstein Condensate. *Phys. Rev. Lett.* **2000**, *84*, 806–809. [[CrossRef](#)]
47. Raman, C.; Abo-Shaer, J.R.; Vogels, J.M.; Xu, K.; Ketterle, W. Vortex Nucleation in a Stirred Bose-Einstein Condensate. *Phys. Rev. Lett.* **2001**, *87*, 210402. [[CrossRef](#)] [[PubMed](#)]
48. Henn, E.A.L.; Seman, J.A.; Roati, G.; Magalhães, K.M.F.; Bagnato, V.S. Generation of Vortices and Observation of Quantum Turbulence in an Oscillating Bose-Einstein Condensate. *J. Low Temp. Phys.* **2009**, *158*, 435. [[CrossRef](#)]
49. Raman, C.; Köhl, M.; Onofrio, R.; Durfee, D.S.; Kuklewicz, C.E.; Hadzibabic, Z.; Ketterle, W. Evidence for a Critical Velocity in a Bose-Einstein Condensed Gas. *Phys. Rev. Lett.* **1999**, *83*, 2502–2505. [[CrossRef](#)]
50. Burger, S.; Bongs, K.; Dettmer, S.; Ertmer, W.; Sengstock, K.; Sanpera, A.; Shlyapnikov, G.V.; Lewenstein, M. Dark Solitons in Bose-Einstein Condensates. *Phys. Rev. Lett.* **1999**, *83*, 5198–5201. [[CrossRef](#)]
51. Caradoc-Davies, B.M.; Ballagh, R.J.; Burnett, K. Coherent Dynamics of Vortex Formation in Trapped Bose-Einstein Condensates. *Phys. Rev. Lett.* **1999**, *83*, 895–898. [[CrossRef](#)]
52. Leanhardt, A.E.; Görlitz, A.; Chikkatur, A.P.; Kielpinski, D.; Shin, Y.; Pritchard, D.E.; Ketterle, W. Imprinting Vortices in a Bose-Einstein Condensate using Topological Phases. *Phys. Rev. Lett.* **2002**, *89*, 190403. [[CrossRef](#)] [[PubMed](#)]
53. Möttönen, M.; Pietilä, V.; Virtanen, S.M.M. Vortex Pump for Dilute Bose-Einstein Condensates. *Phys. Rev. Lett.* **2007**, *99*, 250406. [[CrossRef](#)] [[PubMed](#)]
54. Xu, Z.F.; Zhang, P.; Raman, C.; You, L. Continuous vortex pumping into a spinor condensate with magnetic fields. *Phys. Rev. A* **2008**, *78*, 043606. [[CrossRef](#)]
55. Allen, L.; Beijersbergen, M.W.; Spreeuw, R.J.C.; Woerdman, J.P. Orbital angular momentum of light and the transformation of Laguerre-Gaussian laser modes. *Phys. Rev. A* **1992**, *45*, 8185–8189. [[CrossRef](#)] [[PubMed](#)]
56. Mukherjee, K.; Majumder, S.; Mondal, P.K.; Deb, B. Interaction of a Laguerre-Gaussian beam with trapped Rydberg atoms. *J. Phys. B At. Mol. Opt. Phys.* **2017**, *51*, 015004. [[CrossRef](#)]
57. Mondal, P.K.; Deb, B.; Majumder, S. Angular momentum transfer in interaction of Laguerre-Gaussian beams with atoms and molecules. *Phys. Rev. A* **2014**, *89*, 063418. [[CrossRef](#)]
58. Bhowmik, A.; Mondal, P.K.; Majumder, S.; Deb, B. Interaction of atom with nonparaxial Laguerre-Gaussian beam: Forming superposition of vortex states in Bose-Einstein condensates. *Phys. Rev. A* **2016**, *93*, 063852. [[CrossRef](#)]
59. Bhowmik, A.; Majumder, S. Tuning of non-paraxial effects of the Laguerre-Gaussian beam interacting with the two-component Bose-Einstein condensates. *J. Phys. Commun.* **2018**, *2*, 125001. [[CrossRef](#)]
60. Das, S.; Bhowmik, A.; Mukherjee, K.; Majumder, S. Transfer of orbital angular momentum superposition from asymmetric Laguerre-Gaussian beam to Bose-Einstein Condensate. *J. Phys. B At. Mol. Opt. Phys.* **2020**, *53*, 025302. [[CrossRef](#)]
61. Tabosa, J.W.R.; Petrov, D.V. Optical Pumping of Orbital Angular Momentum of Light in Cold Cesium Atoms. *Phys. Rev. Lett.* **1999**, *83*, 4967–4970. [[CrossRef](#)]
62. He, H.; Friese, M.E.J.; Heckenberg, N.R.; Rubinsztein-Dunlop, H. Direct Observation of Transfer of Angular Momentum to Absorptive Particles from a Laser Beam with a Phase Singularity. *Phys. Rev. Lett.* **1995**, *75*, 826–829. [[CrossRef](#)]
63. Kanamoto, R.; Wright, E.M.; Meystre, P. Quantum dynamics of Raman-coupled Bose-Einstein condensates using Laguerre-Gaussian beams. *Phys. Rev. A* **2007**, *75*, 063623. [[CrossRef](#)]
64. DeMarco, M.; Pu, H. Angular spin-orbit coupling in cold atoms. *Phys. Rev. A* **2015**, *91*, 033630. [[CrossRef](#)]
65. Chen, L.; Pu, H.; Zhang, Y. Spin-orbit angular momentum coupling in a spin-1 Bose-Einstein condensate. *Phys. Rev. A* **2016**, *93*, 013629. [[CrossRef](#)]
66. Nandi, G.; Walser, R.; Schleich, W.P. Vortex creation in a trapped Bose-Einstein condensate by stimulated Raman adiabatic passage. *Phys. Rev. A* **2004**, *69*, 063606. [[CrossRef](#)]
67. Simula, T.P.; Nygaard, N.; Hu, S.X.; Collins, L.A.; Schneider, B.I.; Mølmer, K. Angular momentum exchange between coherent light and matter fields. *Phys. Rev. A* **2008**, *77*, 015401. [[CrossRef](#)]
68. Law, K.J.H.; Kevrekidis, P.G.; Tuckerman, L.S. Stable Vortex-Bright-Soliton Structures in Two-Component Bose-Einstein Condensates. *Phys. Rev. Lett.* **2010**, *105*, 160405. [[CrossRef](#)]
69. Jain, P.; Boninsegni, M. Quantum demixing in binary mixtures of dipolar bosons. *Phys. Rev. A* **2011**, *83*, 023602. [[CrossRef](#)]
70. Roy, A.; Angom, D. Thermal suppression of phase separation in condensate mixtures. *Phys. Rev. A* **2015**, *92*, 011601. [[CrossRef](#)]
71. Andersen, M.F.; Ryu, C.; Cladé, P.; Natarajan, V.; Vaziri, A.; Helmerson, K.; Phillips, W.D. Quantized Rotation of Atoms from Photons with Orbital Angular Momentum. *Phys. Rev. Lett.* **2006**, *97*, 170406. [[CrossRef](#)] [[PubMed](#)]
72. Ramanathan, A.; Wright, K.C.; Muniz, S.R.; Zelan, M.; Hill, W.T.; Lobb, C.J.; Helmerson, K.; Phillips, W.D.; Campbell, G.K. Superflow in a Toroidal Bose-Einstein Condensate: An Atom Circuit with a Tunable Weak Link. *Phys. Rev. Lett.* **2011**, *106*, 130401. [[CrossRef](#)] [[PubMed](#)]
73. Wright, K.; Leslie, L.; Bigelow, N. Optical control of the internal and external angular momentum of a Bose-Einstein condensate. *Phys. Rev. A* **2008**, *77*, 041601(R). [[CrossRef](#)]
74. Kamsap, M.R.; Ekogo, T.B.; Pedregosa-Gutierrez, J.; Hagel, G.; Houssin, M.; Morizot, O.; Knoop, M.; Champenois, C. Coherent internal state transfer by a three-photon STIRAP-like scheme for many-atom samples. *J. Phys. B At. Mol. Opt. Phys.* **2013**, *46*, 145502. [[CrossRef](#)]
75. Wright, E.M.; Arlt, J.; Dholakia, K. Toroidal optical dipole traps for atomic Bose-Einstein condensates using Laguerre-Gaussian beams. *Phys. Rev. A* **2000**, *63*, 013608. [[CrossRef](#)]

76. Timmermans, E. Phase Separation of Bose-Einstein Condensates. *Phys. Rev. Lett.* **1998**, *81*, 5718–5721. [[CrossRef](#)]
77. Wen, L.; Liu, W.M.; Cai, Y.; Zhang, J.M.; Hu, J. Controlling phase separation of a two-component Bose-Einstein condensate by confinement. *Phys. Rev. A* **2012**, *85*, 043602. [[CrossRef](#)]
78. Vudragović, D.; Vidanović, I.; Balaž, A.; Muruganandam, P.; Adhikari, S.K. C programs for solving the time-dependent Gross–Pitaevskii equation in a fully anisotropic trap. *Comput. Phys. Commun.* **2012**, *183*, 2021. [[CrossRef](#)]
79. Egorov, M.; Opanchuk, B.; Drummond, P.; Hall, B.V.; Hannaford, P.; Sidorov, A.I. Measurement of s-wave scattering lengths in a two-component Bose-Einstein condensate. *Phys. Rev. A* **2013**, *87*, 053614. [[CrossRef](#)]
80. Mertes, K.; Merrill, J.; Carretero-Gonzalez, R.; Frantzeskakis, D.; Kevrekidis, P.; Hall, D. Nonequilibrium Dynamics and Superfluid Ring Excitations in Binary Bose-Einstein Condensates. *Phys. Rev. Lett.* **2007**, *99*, 190402. [[CrossRef](#)] [[PubMed](#)]
81. Pethick, C.J.; Smith, H. *Bose-Einstein Condensation in Dilute Gases*; Cambridge University Press: Cambridge, UK, 2002.
82. Stringari, S.; Pitaevskii, L. *Bose-Einstein Condensation*; Oxford University Press: Oxford, UK, 2003.
83. Tojo, S.; Taguchi, Y.; Masuyama, Y.; Hayashi, T.; Saito, H.; Hirano, T. Controlling phase separation of binary Bose-Einstein condensates via mixed-spin-channel Feshbach resonance. *Phys. Rev. A* **2010**, *82*, 033609. [[CrossRef](#)]
84. Trippenbach, M.; Góral, K.; Rzazewski, K.; Malomed, B.; Band, Y.B. Structure of binary Bose-Einstein condensates. *J. Phys. B At. Mol. Opt. Phys.* **2000**, *33*, 4017. [[CrossRef](#)]
85. Ding, D.S.; Zhang, W.; Zhou, Z.Y.; Shi, S.; Xiang, G.Y.; Wang, X.S.; Jiang, Y.K.; Shi, B.S.; Guo, G.C. Quantum Storage of Orbital Angular Momentum Entanglement in an Atomic Ensemble. *Phys. Rev. Lett.* **2015**, *114*, 050502. [[CrossRef](#)] [[PubMed](#)]
86. Hu, Y.X.; Miniatura, C.; Grémaud, B. Half-skyrmion and vortex-antivortex pairs in spinor condensates. *Phys. Rev. A* **2015**, *92*, 033615. [[CrossRef](#)]
87. Semenoff, G.W.; Zhou, F. Discrete Symmetries and $1/3$ -Quantum Vortices in Condensates of $F = 2$ Cold Atoms. *Phys. Rev. Lett.* **2007**, *98*, 100401. [[CrossRef](#)]
88. Nayak, C.; Simon, S.H.; Stern, A.; Freedman, M.; Das Sarma, S. Non-Abelian anyons and topological quantum computation. *Rev. Mod. Phys.* **2008**, *80*, 1083–1159. [[CrossRef](#)]